
Discovering Bugs in Vision Models using Off-the-shelf Image Generation and Captioning

Olivia Wiles^{*1} Isabela Albuquerque¹ Sven Gowal^{*1}

Abstract

Discovering failures in vision classifiers under real-world settings remains an open challenge. This work shows how off-the-shelf, large-scale, image-to-text and text-to-image models, trained on vast amounts of data, can be leveraged to automatically find such failures. In essence, a conditional text-to-image generative model is used to generate large amounts of synthetic, yet realistic, inputs given a ground-truth label. A captioning model is used to describe misclassified inputs and descriptions are used in turn to generate more inputs, thereby assessing whether specific descriptions induce more failures than expected. As failures are grounded to natural language, we automatically obtain a high-level, human-interpretable explanation of each failure. We use this pipeline to interrogate classifiers trained on IMAGENET to find specific failure cases and discover spurious correlations. Discovered failures generalize to other generative models and real images retrieved using *Google Image Search*. We also demonstrate the scalability of our approach by generating large adversarial datasets targeting specific classifier architectures. Finally, we discuss a number of further challenges. Overall, this work demonstrates the potential of large-scale generative models to automatically discover bugs in vision models in an open-ended manner.

1. Introduction

Deep learning has enabled breakthroughs in a wide variety of fields (Goodfellow et al., 2016; Krizhevsky et al., 2012; Hinton et al., 2012), and deep neural networks are ubiquitous in many applications, including autonomous driving (Bojarski et al., 2016) and medical imaging (De Fauw et al., 2018). Unfortunately, these models are known to exhibit numerous failures arising from using *shortcuts* and

^{*}Equal contribution ¹DeepMind, London, UK. Correspondence to: <oawiles,sgowal,isabelaa@google.com>.

Preprint.



Figure 1. Examples of automatically found failures. The correct label is to the left in green. The incorrect prediction is to the right in red. Images are not watermarked upon classification.

spurious correlations (Geirhos et al., 2020a; Arjovsky et al., 2019; Torralba et al., 2011; Kuehlkamp et al., 2017). As a result, they can fail when training and deployment data differ (Buolamwini & Gebru, 2018). Hence, it is important to ensure that models are robust and generalize to new deployment settings. Yet, only a few tools exist to automatically find failure cases on unseen data. Some methods analyze the performance of models by collecting new datasets (usually by scraping the web). These datasets must be large enough to obtain some indication of how models perform on a particular subset of inputs (Hendrycks et al., 2019; 2020; Recht et al., 2019). Other methods rely on expertly crafted, synthetic (and often unrealistic) datasets that highlight particular shortcomings (Geirhos et al., 2022; Xiao et al., 2020).

We present a methodology to automatically find failure cases (see Fig. 1 for some examples) of image classifiers in an open-ended manner, without prior assumptions on the types of failures and how they arise. We leverage off-the-shelf, large-scale, text-to-image, generative models, such as

DALL·E 2 (Ramesh et al., 2022), IMAGEN (Saharia et al., 2022) or STABLE-DIFFUSION (Rombach et al., 2022), to obtain realistic images that can be reliably manipulated using a text prompt. We leverage captioning models, such as FLAMINGO (Alayrac et al., 2022) or LEMON (Hu et al., 2021), to retrieve human-interpretable descriptions of each failure case. This provides the following advantages: (i) generative models trained on web-scale datasets can be re-used and have broad non-domain-specific coverage; (ii) they demonstrate basic compositionality, can generate novel data and can faithfully capture the essence of (most) prompts, thereby allowing images to be realistically manipulated; (iii) textual descriptions of these systematic failures that can be easily interpreted (even by non-experts) and interrogated (e.g., by performing counterfactual analyses). Overall, our contributions are as follows:

- We describe a methodology to discover failures of classifiers trained on IMAGENET (Deng et al., 2009). To the contrary of prior work, we leverage off-the-shelf generative models, thereby avoiding the need to collect new datasets or rely on manually crafted synthetic images.
- Our approach surfaces failures that are human-interpretable by clustering and captioning inputs on which classifiers fail. These captions can be modified to produce alternative hypotheses of why failures occur allowing insights into the limitations of a given model. Furthermore, as failures are grounded to language, we demonstrate that they generalize across multiple text-to-image models and, more importantly, we show that similar failures occur with real images obtained via *Google Image Search*.
- We demonstrate the scalability of the approach by generating adversarial datasets (akin to IMAGENET-A; Hendrycks et al., 2019). In contrast to IMAGENET-A, our new generated datasets align more closely with the original training distribution from IMAGENET and generalize to multiple classifier architectures.

Importantly, while this work focuses on vision models trained on IMAGENET, it is neither limited to IMAGENET nor the visual domain. It serves as a proof-of-concept that demonstrates how large-scale, off-the-shelf, generative models (Bommasani et al., 2021) can be combined to automate the discovery of *bugs* in machine learning models and produce compelling, interpretable descriptions of model failures. The approach is agnostic to the model architecture, which can be treated as a black box.

2. Related Work

Model failures. Spurious correlations can entice models to learn unintended shortcuts that obtain high accuracy on the training set but fail to generalize to new settings (Lapuschkin et al., 2019; Geirhos et al., 2020a). Recht et al.

(2019) show that the accuracy of IMAGENET models is impacted by changes in the data collection process, while Torralba et al. (2011); Khosla et al. (2012); Choi et al. (2012) explore how contextual bias affects generalization. Mania et al. (2019) demonstrate that models trained on IMAGENET make consistent mistakes with one another and Geirhos et al. (2020b) show that these mistakes are not necessarily consistent with human judgment.

Evaluation datasets. Understanding how model failures arise and empirically analyzing their consequences often requires collecting and annotating new test datasets. Hendrycks et al. (2019) collected datasets of natural adversarial examples (IMAGENET-A and IMAGENET-O) to evaluate how model performance degrades when inputs have limited spurious cues. Hendrycks et al. (2020) collected four real-world datasets (including IMAGENET-R) to understand how models behave under distribution shifts. In many cases, particular shortcomings can only be explored using synthetic datasets (Cimpoi et al., 2013). Hendrycks & Dieterich (2018) introduced IMAGENET-C, a synthetic set of common corruptions. Geirhos et al. (2018) propose to use images with a texture-shape cue conflict to evaluate the propensity of models to over-emphasize texture cues. Xiao et al. (2020); Sagawa et al. (2020) investigate whether models are biased towards background cues by compositing foreground objects with various background images (IMAGENET-9, WATERBIRDS). In all cases, building such datasets is time-consuming and requires expert knowledge.

Automated failure discovery. In some instances, it is possible to distill rules or specifications that constrain the input space enough to enable the automated discovery of failures via optimization or brute-force search. In vision tasks, adversarial examples, which are constructed using ℓ_p -norm bounded perturbations of the input, can cause neural networks to make incorrect predictions with high confidence (Carlini & Wagner, 2017a;b; Goodfellow et al., 2014; Kurakin et al., 2016; Szegedy et al., 2013). In language tasks, some efforts manually compose templates to generate test cases for specific failures (Jia & Liang, 2017; Garg et al., 2019; Ribeiro et al., 2020). Such approaches rely on human creativity and are intrinsically difficult to scale. Several works (Baluja & Fischer, 2017; Song et al., 2018; Xiao et al., 2018; Qiu et al., 2019; Wong & Kolter, 2021; Laidlaw et al., 2020; Goyal et al., 2019) go beyond hard-coded rules by leveraging generative and perceptual models. However, such approaches are difficult to automate as it is unclear how to relate specific latent variables to isolated structures of the original input. Finally, we highlight a concurrent work (Ge et al., 2022), which leverages captioning and text-to-image models to construct background images to evaluate (and improve) an object detector. Their approach requires compositing the resulting images with foreground objects and is not open-ended, in the sense that it requires a dataset

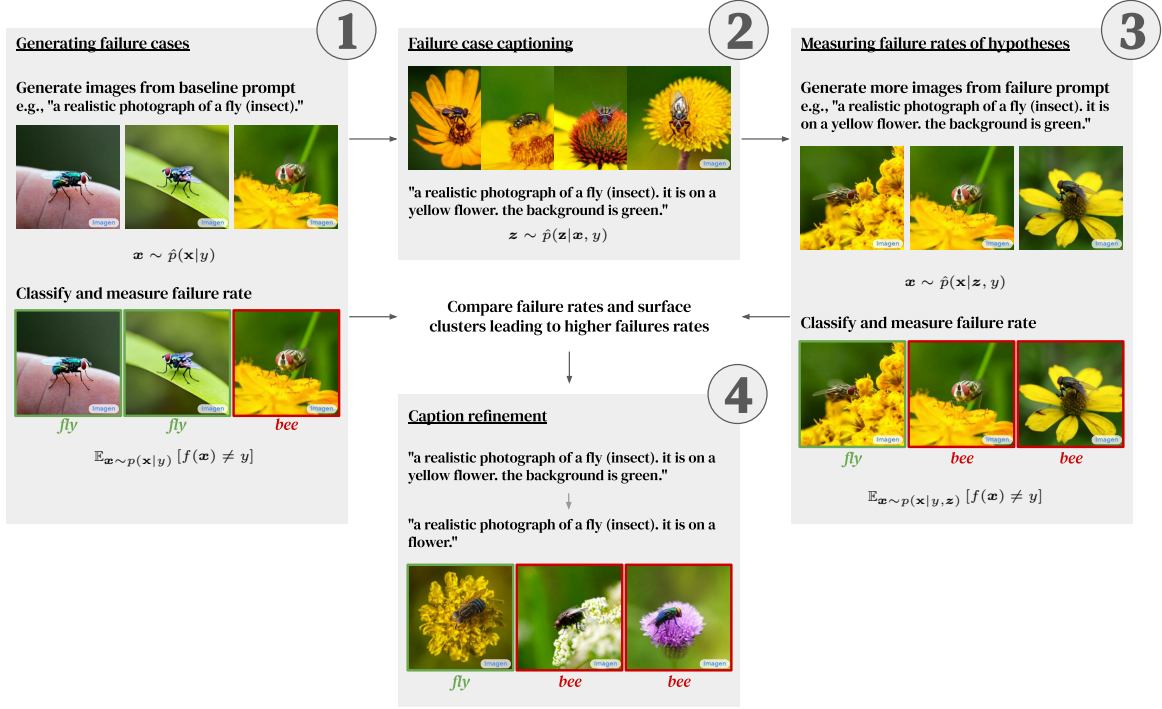


Figure 2. **Diagram of our method.** The method starts by generating images containing a given class y to measure the baseline failure rate of that class (right-hand side of Eq. 1). We construct a textual description for each misclassified image. This description is used to produce new images and measure the failure rate on images corresponding to that description (left-hand side of Eq. 1). The final description can be edited (manually or automatically) to understand the source of the failures.

of background images. Perhaps, the work by Perez et al. (2022) on *red-teaming* language models is the most similar to ours. Perez et al. demonstrate how to prompt a language model to automatically generate test cases to probe another language model for toxic and other unintended output.

Interpretability. Interpretability techniques aim to give a rationale behind individual model predictions. Casper et al. (2022) demonstrate that feature-level attacks, which create adversarial patches, can help diagnose brittle feature associations. However, much like LIME (Ribeiro et al., 2016) or GRAD-CAM (Selvaraju et al., 2019), the results are difficult to understand. Other works (Abid et al., 2022; Jain et al., 2022a; Eyuboglu et al., 2022) leverage auxiliary information in the form of attributes or image-to-text embeddings (e.g., from CLIP; Radford et al., 2021) to provide explanations in natural language. However, these methods often rely on an additional dataset which limits their scope.

3. Method

Notation. We consider a classifier $f : \mathbb{X} \rightarrow \mathbb{Y}$, where \mathbb{X} is the set of inputs (i.e., images) and \mathbb{Y} is the label set. We also assume that inputs $x \in \mathbb{X}$ with label $y \in \mathbb{Y}$ are drawn from an underlying distribution $p(x|z, y)$ conditioned on latent representations $z \in \mathbb{Z}$. In the context of this specific

work, z is a textual description of the image x . We are interested in discovering captions z corresponding to images $x \sim p(x|z, y)$ with label y that lead to significantly higher misclassification rates than generic images drawn from the marginal distribution $p(x|y)$ conditioned solely on the label. Formally, given a label y , we would like to find z with

$$\mathbb{E}_{x \sim p(x|z, y)} [f(x) \neq y] > \mathbb{E}_{x \sim p(x|y)} [f(x) \neq y] \quad (1)$$

where $[\cdot]$ represents the Iverson bracket. We may also be interested in identifying specific misclassifications towards a wrong (target) label $\bar{y} \neq y$, and would like that

$$\mathbb{E}_{x \sim p(x|z, y)} [f(x) = \bar{y}] > \mathbb{E}_{x \sim p(x|y)} [f(x) = \bar{y}]. \quad (2)$$

As we do not have access to the true underlying distributions $p(x|z, y)$ and $p(x|y)$, we leverage a large-scale text-to-image model, IMAGEN, to approximate them. Similarly, we approximate $p(z|x, y)$ with a captioning model, FLAMINGO. We denote approximations of these distributions with the symbol \hat{p} .

For each of the following steps, we highlight additional

implementation details and explain how we construct prompts for the text-to-image and image-to-text models.

Generating failure cases. Our approach is described in Fig. 2. It consists of initially finding *baseline* failures for the underlying model f by sampling inputs \mathbf{x} from $\hat{p}(\mathbf{x}|y)$.¹ Given a label of interest y , the output of this step is a set $\mathbb{D} = \{\mathbf{x}_i \sim \hat{p}(\mathbf{x}|y)\}_{i=1}^N$ (where N is the number of images we wish to generate), a set $\mathbb{D}_{\text{fail}} = \{\mathbf{x} \in \mathbb{D} | f(\mathbf{x}) \neq y\}$ and an estimate of the baseline failure rate $|\mathbb{D}_{\text{fail}}|/N$ (corresponding to the right-hand side of Eq. 1). In this work, we consider problematic misclassifications only so we restrict ourselves to failures where any of the top-3 predicted labels are not under the same parent as the true label y in the WORDNET hierarchy (Miller, 1995).²

This step leverages a text-to-image generative model conditioned on y with prompts such as “*a realistic photograph of a fly (insect).*”, which are automatically generated from the corresponding class and WORDNET hierarchy. As our domain of interest is composed of real images, the prompt is designed to enforce the generation of photographs of real objects and animals rather than drawings or paintings. Further prompt engineering can be explored to find failures on a variety of domains (such as sketches or medical imaging; Hendrycks et al., 2020; Kather et al., 2022).

Optional clustering failure cases. Clustering is not necessary, but makes the search for the caption \mathbf{z} leading to high failure rates more efficient and computationally manageable. First, we split \mathbb{D}_{fail} by predicted label, i.e. $\mathbb{D}_{\text{fail}} = \mathbb{D}_{\text{fail}}^{(1)} \cup \dots \cup \mathbb{D}_{\text{fail}}^{(|\mathcal{Y}|)}$, where $\mathbb{D}_{\text{fail}}^{(y)} = \{\mathbf{x} \in \mathbb{D}_{\text{fail}} | f(\mathbf{x}) = y\}$. Then, for each subset $\mathbb{D}_{\text{fail}}^{(y)}$, we group inputs that have similar feature representations together (e.g., using the cosine distance between intermediate activations of a pretrained model). The goal of this step is to reduce the number of clusters to a minimum without amalgamating different causes of failure together.³

Failure case captioning. For each cluster $\mathbb{A} \subseteq \mathbb{D}_{\text{fail}}$, we would like to find a caption $\mathbf{z}_{\mathbb{A}}$ that describes it. Grounding failures in simple textual descriptions allows us to maintain

¹In practice, it is possible to steer the generation process to induce more frequent failures (e.g., by optimizing latents or conditioning via gradient ascent on the cross-entropy loss; Wong & Kolter, 2021). However, as a proof-of-concept, we assume only black-box access to off-the-shelf text-to-image model.

²Other options include considering only misclassifications where the true label is not in the top- k predicted labels or where the confidence in the true label is lower than a predefined threshold.

³Wrongful clustering may lead the next step to produce descriptions that fail to induce more failures. As a result, we may miss failures that we would have discovered without clustering, but the failures that we do discover remain valid.

the diversity of the generated images: the generated images resemble the images leading to the original failure without being exact copies. Ideally, we would like to find the caption $\mathbf{z}_{\mathbb{A}}$ that maximizes the likelihood of sampling elements of \mathbb{A} , i.e., $\mathbf{z}_{\mathbb{A}} = \arg \max_{\mathbf{z}} \prod_{\mathbf{x} \in \mathbb{A}} \hat{P}(\mathbf{x}|\mathbf{z}, y)$. We may wish to impose constraints on $\mathbf{z}_{\mathbb{A}}$, such as a maximum number of words or sentences.⁴ Finding such a caption is computationally hard and measuring exact likelihoods $\hat{P}(\mathbf{x}|\mathbf{z}, y)$ can be challenging. Hence, we resort to sampling captions directly from a captioning model $\hat{p}(\mathbf{z}|\mathbf{x}, y)$ for each image of cluster \mathbb{A} .⁵ Captions are split into sentences, resulting in a set of sentences \mathbb{S} . Sentences are greedily combined (up to a maximum number of sentences K) to maximize the likelihood of sampling the overall caption $\mathbf{z}_{\mathbb{A}} = [s_1, \dots, s_K]$ with $s_j = \arg \max_{s \in \mathbb{S}} \prod_{\mathbf{x} \in \mathbb{A}} \hat{P}([s_1, \dots, s_{j-1}, s]|\mathbf{x}, y)$ and $s_1 = \arg \max_{s \in \mathbb{S}} \prod_{\mathbf{x} \in \mathbb{A}} \hat{P}([s]|\mathbf{x}, y)$. If no clustering is performed, we can directly sample a caption $\mathbf{z}_{\{\mathbf{x}\}} \sim \hat{p}(\mathbf{z}|\mathbf{x}, y)$ from the captioning model for each element \mathbf{x} in \mathbb{D}_{fail} . Each caption serves as a failure hypothesis.

This step leverages an image-to-text captioning model and forces descriptive completions via few-shot prompting. In particular, we use three shots, with each shot being an image and caption pair. Images are publicly available online and are manually described using between four to seven short sentences that describe the subject of the photograph and its physical position with respect to the camera, as well as the background or context in which the subject appears (see Appendix A for more details). To condition on y , we force the captioning model to only consider completions to the original baseline prompt, which guarantees that the final caption contains the true label. An example of a resulting caption is “*a realistic photograph of a fly (insect). the background is blurred. the fly is in focus. it is on a yellow flower. the background is green.*” Each caption serves as a failure hypothesis.

Measuring failure rates of hypotheses. For each failure hypothesis or caption $\mathbf{z}_{\mathbb{A}}$, we can measure its failure rate via sampling $\mathbb{E}_{\mathbf{x} \sim p(\mathbf{x}|\mathbf{z}_{\mathbb{A}}, y)} [f(\mathbf{x}) \neq y]$. This step allows us to surface captions \mathbf{z}^* that satisfy Eq. 1 (or alternatively Eq. 2) by comparing the resulting failure rate with the baseline failure rate obtained initially.

This step uses the text-to-image model, which we now prompt with descriptive cluster captions, e.g. “*a realistic photograph of a fly (insect). the background is blurred. the fly is in focus. it is on a yellow flower. the background*

⁴These constraints guarantee that captions remain simple and not overly descriptive.

⁵This formulation implicitly assumes that any caption is as likely as another under a given label y , which in general does not hold true, but serves as a reasonable approximation.

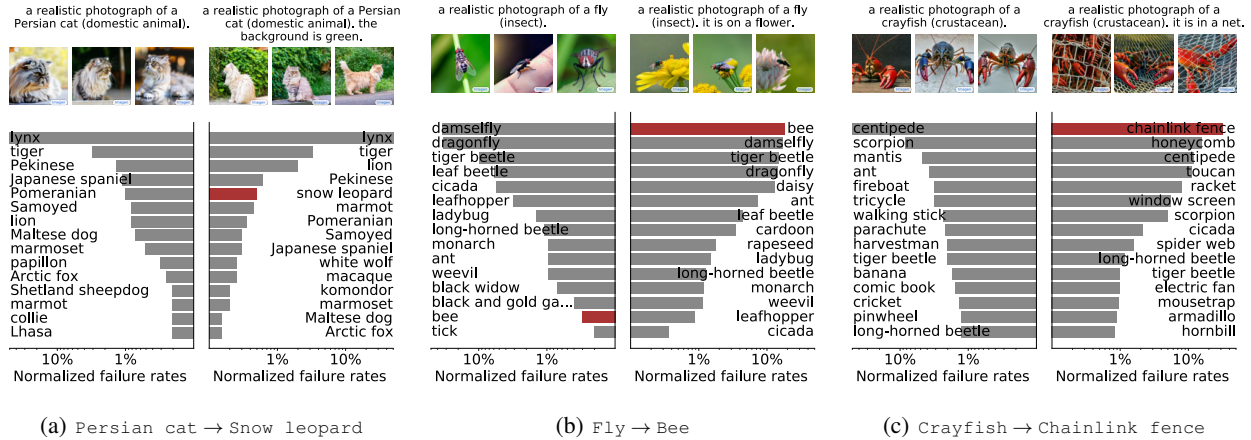


Figure 3. Distribution of failures of a RESNET-50 for the baseline and automatically discovered captions for three true and target label pairs. For each panel, failures resulting from the baseline caption are on the left and failures resulting from the discovered caption are on the right. We show the top-15 mistakes and three randomly sampled images for each caption. We highlight in red the bar corresponding to the target label. Absolute failure rates are given in Table 1.

is green.”

Caption refinement and counterfactual analysis.

Given a caption z^* , we want to provide a shorter, self-contained caption that obtains a similar failure rate. For this step, we rely on simple rules⁶ and evaluate promising caption rewrites. Finally, as captions are human-readable, users can interact with the system and test alternative hypotheses.

In our implementation, we exploit two rules: (i) we evaluate all individual sentences (for our ongoing example, these would be “the background is blurred”, “the fly is in focus”, “it is on a yellow flower” and “the background is green”) in conjunction with the original prompt (e.g., “a realistic photograph of a fly (insect)”); (ii) the most promising prompt is further refined by dropping adjectives (such as “yellow” in “it is on a yellow flower”). More sophisticated rules and rewrites are possible (Ribeiro et al., 2018). Alternatively, we could leverage a large-language model via few-shot prompting to automate this process (Witteveen & Andrews, 2019).

Finally, we note that it is possible to use part of this pipeline to understand known failure cases (e.g., on failures reported by external users of the model f).

⁶This may seem at odds with our claim on open-endedness. However, we note that this step is optional and its goal is simply to produce shorter failure descriptions.

4. Results

We elaborate on two use-cases. First, we find failure cases of a Residual Network (RESNET)-50 (He et al., 2016) trained on IMAGENET. We focus on three arbitrarily chosen labels and show that the failures we obtain arise from consistent misclassifications caused by spurious correlations. We show that these failures generalise to *real* images downloaded through *Google Image Search*. Second, we generate failures at scale for various models and show that these failures generalise to other architectures and model initializations.

4.1. Open-ended failure search

Setup. We evaluate a RESNET-50 trained on IMAGENET and available on TF-HUB.⁹ We select three labels y at random: Persian cat, fly and crayfish. For each label y , we manually select target labels \bar{y} (snow leopard, bee and chainlink fence respectively) and execute the protocol defined in Sec. 3. At each step, we sample images from the generative model until we gather 20 images that are misclassified as the target label \bar{y} and compute failure rates at that point. Fig. 3 and Table 1 show these automatically discovered failures. More failures for additional true and target label pairs are in Sec. B.1 in the appendix. In Sec. B.1, we also evaluate other architectures (i.e., VITs) and demonstrate that the discovered captions yield failure rates that are statistically significant.

Discovered failures. Fig. 3(a) shows the distribution of failures for the baseline label Persian cat. We observe

⁹https://tfhub.dev/google/imagenet/resnet_v2_50/classification/5

Discovering Bugs in Vision Models using Off-the-shelf Image Generation and Captioning

True label	Target label	Caption	Failure rate (any)		Failure rate (target)	
Persian cat	Snow leopard	a realistic photograph of a Persian cat (domestic animal).	0.11%	1×	0.00022%	1×
		— ” — the background is green.	0.64%	6×	0.0032%	14×
Fly	Bee	a realistic photograph of a fly (insect).	0.48%	1×	0.0014%	1×
		— ” — it is on a flower.	4.11%	9×	0.72%	497×
Crayfish	Chainlink fence	a realistic photograph of a crayfish (crustacean).	0.93%	1×	0.00047%	1×
		— ” — it is in a net.	6.31%	7×	1.73%	3721×

Table 1. **Absolute failure rates of a RESNET-50 for three true and target label pairs.** We show the total failure rate (i.e., the model prediction is different from the true label) and the target failure rate (i.e., the model prediction is the target label). Captions are automatically discovered using the method detailed in Sec. 3.⁸

that the most frequent confusion, on images generated using the baseline caption “*a realistic photograph of a Persian cat (domestic animal).*” is with `lynx`. This mistake arises about 0.1% of the time and constitutes 87.3% of all failures. In comparison, the confusion with `snow leopard` is rather infrequent and arises only 0.00022% of the time. Our approach automatically discovers that adding “*the background is green.*” to the caption results in a large increase in failure rates. Failures are 5.72× more likely and the model is 14.3× more likely to predict `snow leopard`. We generally observe that mistakes with wild animals become more prevalent when the cat is outdoors. Similarly, Fig. 3(b) and Fig. 3(c) show failures on images of flies and crayfish, respectively. Flies on flowers are significantly more likely to be confused for bees when they are on flowers (497×), while crayfish in nets are more frequently confused as chainlink fences (3721×), honeycomb, window screens or spider webs. These highlight two shortcomings of the underlying classifier: (i) the over-reliance on spurious cues (such as the flower); (ii) the inability to determine which object is the main subject of a photograph (e.g., which of the net or crayfish is important).

Generalization of failure descriptions. To verify that the discovered failures are not specific to the text-to-image model used in this manuscript and do not result from artifacts in the image generation process, we generate 30 images using the baseline and discovered captions with DALL·E 2 and STABLE-DIFFUSION (samples are shown in Fig. 13 and Fig. 14 in the appendix). We evaluate the failure rates for the `fly` and `crayfish` labels (which exhibited higher failure rates). With DALL·E 2, for the 30 images generated with the prompt “*a realistic photograph of a fly*

⁹As a point of comparison, we can also evaluate the baseline failure rates on images from the IMAGENET test set. For `Persian cat`, `fly` and `crayfish` the baseline failure rates are 16%, 8% and 18%, respectively (the target failure rate is 0% for all labels). These failure rates are higher than on images generated by the generative model, this is perhaps indicating that the generative model produces images that are more canonical and conservative. We also point out that we generate 9.1M samples to compute the first row of the table, 625K for the second and 1.4M, 2.8K, 4.3M, 1.2K for the subsequent rows.

(*insect*).”, 18 are correctly classified as flies and none as bees. When adding “*it is on a flower.*” to the prompt, the overall failure rate increases (only 14 images are correctly classified) and nine images are now classified as bees. Similarly, for “*a realistic photograph of a crayfish (crustacean).*”, 29 images are correctly classified as `crayfish`, `spiny lobster`, `American lobster`, `Dungeness crab` or `king crab`, while none are classified as `chainlink fence`. When adding “*it is in a net.*”, four are classified as `chainlink fence` (with `chainlink fence` appearing ten times in the top-3 predictions), while only 21 images are correctly classified. Results are similar for STABLE-DIFFUSION images.¹⁰ Overall, we observe that discovered failures generalize across generative models.

Generalization to Google Image Search. Finally, we verify that failures generalise to images queried through *Google Image Search*¹¹. We query *Google Image Search* to find 30 images for each of the following queries: “*fly*”, “*fly on flower*”, “*crayfish*”, “*crayfish in net*” (images must have a resolution of at least 256×256 and should contain the true label). We classify all images and observe that the number of failures towards `bee` increases from zero to two and those towards `chainlink fence` increase from zero to four. This illustrates that the discovered failures are general and even extend to real photographs. Further examples are given in Sec. B.1.

4.2. Adversarial dataset generation at scale

We demonstrate how to apply our automated pipeline to generate large datasets of failures. We seed our search by captioning images from IMAGENET-A. We show that the discovered failures generalize across initializations of a given model architecture and between models of different architectures.

Generating large-scale datasets. We assume that we have access to a set of captions that describe potential failure

¹⁰The number of failures increases from one to two and from four to 16, for the `fly` and `crayfish` labels respectively.

¹¹<https://images.google.com>

IN-G-RN1	39%	53%	46%	63%	69%	71%	100%	78%	59%	54%
IN-G-VIT1	50%	61%	55%	69%	74%	76%	79%	77%	100%	77%
ImageNet	5%	8%	9%	13%	14%	12%	11%	10%	6%	6%
	VIT-B/16	VIT-B/32	BIT-M (101x1)	BIT-S (101x1)	Inception V3	ResNet152-V2	RN1	RN2	VIT1	VIT2

Figure 4. **Failure rates (top-3) for different models on two generated datasets and IMAGENET.** We report the failure rates of different models trained on IMAGENET .

cases.¹² These captions are automatically extracted from the 7,500 images of IMAGENET-A using the captioning model, limiting its output to two sentences maximum. For each caption, we sample up to a thousand images keeping those leading to misclassifications and limit the number of misclassified images kept per caption. We consider two models: a RESNET-50 (abbreviated hereafter by RN) and a Vision Transformer in its B/16 variant (Dosovitskiy et al., 2020), abbreviated by VIT. Both models are trained solely on IMAGENET and achieve 76% and 80% top-1 accuracy, respectively. This yields two separate datasets of failures which we refer to as IN-G-RN and IN-G-VIT that are of size 12,332 and 9,536 respectively.

Visualizations of failure cases. Fig. 1 shows samples from IN-G-RN with true and predicted labels. While the images clearly show the correct class, the model erroneously predicts a different one. Additional samples for IN-G-RN and IN-G-VIT are in Fig. 15 and Fig. 16 (in the appendix). Appendix C provides an analysis for some failure cases found in IN-G-VIT and details how images from the IMAGENET training set may have misled the classifier.

Generalization to other networks. We verify that our failures generalize to new architectures and initializations of a specific model to demonstrate that the failures are general and robust. We train an additional RESNET (RN2) and VIT (VIT2) on IMAGENET with the same setup as our two original models but different random seeds. We also consider a large set of additional models trained on IMAGENET and optionally pre-trained on larger datasets obtained from TF-HUB. Fig. 4 shows the failure rates induced by both datasets on all models (failures are accounted when the top-3 predictions do not include the true label). First, we observe that failures transfer well between models of the same architecture. Indeed, 78% of the failures in IN-G-RN

¹²This assumption is not necessary. However, it accelerates our search by generating images that are more likely to induce failures.

Dataset	FID ↓	KID ↓
IMAGENET-A	56.6	0.0460
IN-G-RN	48.3	0.0305
IN-G-VIT	53.9	0.0330
IMAGENET (train)	2.3	0.0003

Table 2. **FID and KID scores.** We report FID and KID scores in relation to IMAGENET (test).

transfer to RN2, while the ones in IN-G-VIT transfer with 77% chance to VIT2. Second, we observe that failures for a given model architecture transfer to a large extent across architectures. Even when large-scale pretraining is used (with the BIT-M (101x1), VIT-B/16 and VIT-B/32 models pretrained on IMAGENET21K), failures transfer at a rate of 39-53% for IN-G-RN and 50-61% for IN-G-VIT. Further results for additional models are in Sec. B.2 in the appendix.

Distribution shift. We compare our generated datasets to IMAGENET and IMAGENET-A to validate that we generate images that are similar to those in IMAGENET. We compute the Fréchet Inception Distance (FID; Heusel et al., 2017) and the Kernel Inception Distance (KID; Binkowski et al., 2018) between the generated images and the IMAGENET test set. Table 2 also shows the FID and KID of the IMAGENET train set and IMAGENET-A. We find that our generated images are *more* similar to those from IMAGENET under both metrics than those from IMAGENET-A.

5. Discussion

Our work demonstrates that today’s large-scale text-to-image and image-to-text models can be leveraged to find human-interpretable failures in vision models. We have demonstrated these failures generalize to real images, other architectures, and can be obtained at scale. While we focus on IMAGENET, there are encouraging signs that generative models could be used to probe models trained on specialized tasks such as medical imaging (Kather et al., 2022). Overall, there remain a number of key challenges to address.

Coverage. While our approach can be used to demonstrate the presence of failures, it is important to note that (just like scraping the web or using a fixed dataset) it cannot prove their absence: there is no guarantee that it will discover all failures of a given model.¹³ Moreover, the generative model is only an approximation of the distribution of interest and may lack coverage. For example, it might almost never generate “a lawnmower falling down from the sky” (an actual image from the IMAGENET training set; Jain et al., 2022b) when prompted with “a realistic photo-

¹³If the generative model matches the true distribution of images, it is possible to give meaningful probabilistic guarantees.

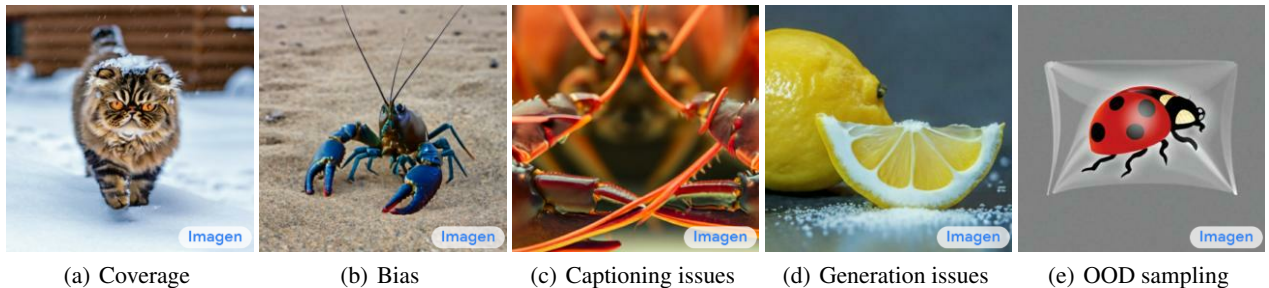


Figure 5. **Illustrative examples of various challenges.** (a) Persian cats in snow (generated using “a realistic photograph of a Persian cat (domestic animal). it is walking in the snow.”) are misclassified as snow leopards at a rate of 0.016%, which is significantly higher than the failure rate of 0.0032% induced by the automatically found caption (“— ” — the background is green.”); the total failure rate also increases twelve-fold to 8.15% (from 0.64%). (b) It is estimated that only 1 in 10,000 crayfish turn blue. However, 9% of the images generated using “a realistic photograph of a crayfish (crustacean).” contain a blue crayfish (estimated by manually looking at 100 samples). (c) This image of a crayfish is misclassified as a chainlink fence. The output of the captioning model for this particular image is “a realistic photograph of a crayfish. the crayfish is very detailed. the crayfish is facing the camera. the crayfish is orange. it has two antennae.” While the caption describes the image, it does not provide enough detail to reconstruct the image. (d) This image is generated from the caption “a realistic photograph of a saltshaker (container). there is a lemon slice on the side of the salt shaker.” While the image contains a lemon, the true class y (saltshaker) is not visible. (e) Generated with the caption “a realistic photograph of a ladybug (insect). it is in a plastic bag.”, this image illustrates that text-to-image models can create image that are not from the intended distribution (i.e., of realistic photographs).

graph of a lawnmower”. While this can help ground failures to scenes that are likely to occur in the real-world, it also means that rare failures are unlikely to be discovered (see Fig. 5(a)).

Bias. While we take the view that off-the-shelf large-scale generative models are trained on diverse and unbiased data, these models mirror the distribution of images and captions seen on the web. The generative model may over-sample particular regions of the image manifold and, as a result, our approach is more likely to discover failures in these high-density regions while missing failures pertaining to other regions (see Fig. 5(b)). (This is similar to how IMAGENET over-represents dogs.) Possible solutions to reduce bias include clever prompting (which introduces expert knowledge) or discovering failure prompts more actively by avoiding random sampling (e.g., through adversarial techniques).

Captioning issues. Using captions allows our approach to produce human-interpretable explanations and constrains our search to failures that can be explained in words. Not only is it possible for the captioning model to miss important details or produce ungrounded captions, but some failures may simply be hard to describe (even by a human). As a result, newly generated images may look different from the set of images that induced the original failure. We note that efficiently enforcing consistency between the generated and original images (through a common caption) is an open problem since we would like to search over *reasonable* captions that are likely to produce images corresponding to the original failure. Fig. 5(c) shows an example where

a crayfish is misclassified as a chainlink fence. While the reason for that failure is immediately obvious to us, it remains difficult to describe with a succinct caption.

Out-of-distribution sampling. Ensuring that images sampled from an off-the-shelf generative model are part of the intended distribution (e.g., resembling IMAGENET) is difficult. We start our prompts with “a realistic photograph” in a bid to help steer the approximated distribution $\hat{p}(x|y, z)$ away from artistic drawings and closer to the true distribution $p(x|y, z)$. This approach is effective (as our images are statistically more similar to IMAGENET than those in IMAGENET-A are as discussed in Fig. 4.2), but not always successful (see Fig. 5(e)). In some cases, finding a suitable prompt is not obvious (e.g., to output images from a particular medical domain; Kather et al., 2022) and fine-tuning models on the dataset of interest may be necessary.

Image generation issues. While the text-to-image model may make occasional mistakes (e.g. generating the wrong object 1.45% of the time for unambiguous prompts – see Sec. B.3), subtle errors can arise. The prompt can be ambiguous due to the presence of homonyms (e.g., a “walking stick” can be both a cane or an insect), or may describe multiple objects with complex relationships that exacerbate mistakes (see Fig. 5(d)).

Privacy. As we are generating large amounts of data, it is important to consider the associated privacy risks. While these risks can be mitigated by using generative models trained on public, non-sensitive data, more research on private generative modelling is necessary (Harder et al., 2022).

Despite these challenges, we foresee that large-scale generative models will increasingly be used as debugging tools. Moreover, as large-scale models improve so will our pipeline. In this work, we introduced an automated pipeline that discovers failure cases in vision models. Our work demonstrates that such a system allows for large-scale investigations of vision models in an open-ended manner as it is automatic and failures are human-intepretable and generalize to other architectures and real images.

References

- Abid, A., Yuksekgonul, M., and Zou, J. Meaningfully debugging model mistakes using conceptual counterfactual explanations. In *International Conference on Machine Learning*. PMLR, 2022.
- Alayrac, J.-B., Donahue, J., Luc, P., Miech, A., Barr, I., Hasson, Y., Lenc, K., Mensch, A., Millican, K., Reynolds, M., Ring, R., Rutherford, E., Cabi, S., Han, T., Gong, Z., Samangoeei, S., Monteiro, M., Menick, J., Borgeaud, S., Brock, A., Nematzadeh, A., Sharifzadeh, S., Binkowski, M., Barreira, R., Vinyals, O., Zisserman, A., and Simonyan, K. Flamingo: a visual language model for few-shot learning. *arXiv preprint arXiv:2204.14198*, 2022.
- Arjovsky, M., Bottou, L., Gulrajani, I., and Lopez-Paz, D. Invariant risk minimization. *arXiv preprint arXiv:1907.02893*, 2019.
- Baluja, S. and Fischer, I. Adversarial transformation networks: Learning to generate adversarial examples. *arXiv preprint arXiv:1703.09387*, 2017.
- Biggio, B., Corona, I., Maiorca, D., Nelson, B., Srndic, N., Laskov, P., Giacinto, G., and Roli, F. Evasion Attacks against Machine Learning at Test Time. *arXiv preprint arXiv:1708.06131*, 2013.
- Binkowski, M., Sutherland, D. J., Arbel, M., and Gretton, A. Demystifying MMD GANs. In *International Conference on Learning Representations*, 2018.
- Bojarski, M., Del Testa, D., Dworakowski, D., Firner, B., Flepp, B., Goyal, P., Jackel, L. D., Monfort, M., Muller, U., Zhang, J., Zhang, X., Zhao, J., and Zieba, K. End to end learning for self-driving cars. *arXiv preprint arXiv:1604.07316*, 2016.
- Bommasani, R., Hudson, D. A., Adeli, E., Altman, R., Arora, S., von Arx, S., Bernstein, M. S., Bohg, J., Bosselut, A., Brunskill, E., Brynjolfsson, E., Buch, S., Card, D., Castellon, R., Chatterji, N., Chen, A., Creel, K., Davis, J. Q., Demszky, D., Donahue, C., Doumbouya, M., Durmus, E., Ermon, S., Etchemendy, J., Ethayarajh, K., Fei-Fei, L., Finn, C., Gale, T., Gillespie, L., Goel, K., Goodman, N., Grossman, S., Guha, N., Hashimoto, T., Henderson, P., Hewitt, J., Ho, D. E., Hong, J., Hsu, K., Huang, J., Icard, T., Jain, S., Jurafsky, D., Kalluri, P., Karamcheti, S., Keeling, G., Khani, F., Khattab, O., Koh, P. W., Krass, M., Krishna, R., Kuditipudi, R., Kumar, A., Ladhak, F., Lee, M., Lee, T., Leskovec, J., Levent, I., Li, X. L., Li, X., Ma, T., Malik, A., Manning, C. D., Mirchandani, S., Mitchell, E., Munyikwa, Z., Nair, S., Narayan, A., Narayanan, D., Newman, B., Nie, A., Niebles, J. C., Nilforoshan, H., Nyarko, J., Ogut, G., Orr, L., Papadimitriou, I., Park, J. S., Piech, C., Portelance, E., Potts, C., Raghunathan, A., Reich, R., Ren, H., Rong, F., Roohani, Y., Ruiz, C., Ryan, J., Ré, C., Sadigh, D., Sagawa, S., Santhanam, K., Shih, A., Srinivasan, K., Tamkin, A., Taori, R., Thomas, A. W., Tramèr, F., Wang, R. E., Wang, W., Wu, B., Wu, J., Wu, Y., Xie, S. M., Yasunaga, M., You, J., Zaharia, M., Zhang, M., Zhang, T., Zhang, X., Zhang, Y., Zheng, L., Zhou, K., and Liang, P. On the opportunities and risks of foundation models. *arXiv preprint arXiv:2108.07258*, 2021.
- Buolamwini, J. and Gebru, T. Gender shades: Intersectional accuracy disparities in commercial gender classification. In *Conference on Fairness, Accountability and Transparency*, 2018.
- Carlini, N. and Wagner, D. Adversarial examples are not easily detected: Bypassing ten detection methods. In *Proceedings of the ACM Workshop on Artificial Intelligence and Security*, 2017a.
- Carlini, N. and Wagner, D. Towards evaluating the robustness of neural networks. In *2017 IEEE Symposium on Security and Privacy*, 2017b.
- Casper, S., Nadeau, M., Hadfield-Menell, D., and Kreiman, G. Robust feature-level adversaries are interpretability tools. *arXiv preprint arXiv:2110.03605*, 2022.
- Choi, M. J., Torralba, A., and Willsky, A. S. Context models and out-of-context objects. *Pattern Recognition Letters*, 2012.
- Cimpoi, M., Maji, S., Kokkinos, I., Mohamed, S., and Vedaldi, A. Describing textures in the wild. *arXiv preprint arXiv:1311.3618*, 2013.
- De Fauw, J., Ledsam, J. R., Romera-Paredes, B., Nikolov, S., Tomasev, N., Blackwell, S., Askham, H., Glorot, X., O’Donoghue, B., Visentin, D., Driessche, G. v. d., Lakshminarayanan, B., Meyer, C., Mackinder, F., Bouton, S., Ayoub, K., Chopra, R., King, D., Karthikesalingam, A., Hughes, C. O., Raine, R., Hughes, J., Sim, D. A., Egan, C., Tufail, A., Montgomery, H., Hassabis, D., Rees, G., Back, T., Khaw, P. T., Suleyman, M., Cornebise, J., Keane, P. A., and Ronneberger, O. Clinically applicable deep learning for diagnosis and referral in retinal disease. In *Nature Medicine*, 2018.

- Deng, J., Dong, W., Socher, R., Li, L.-J., Li, K., and Fei-Fei, L. Imagenet: A large-scale hierarchical image database. In *Proceedings of the IEEE/CVF Conference on Computer Vision and Pattern Recognition*, 2009.
- Dosovitskiy, A., Beyer, L., Kolesnikov, A., Weissenborn, D., Zhai, X., Unterthiner, T., Dehghani, M., Minderer, M., Heigold, G., Gelly, S., Uszkoreit, J., and Houslyby, N. An Image is Worth 16x16 Words: Transformers for Image Recognition at Scale. *arXiv preprint arXiv:2010.11929*, 2020.
- Eyuboglu, S., Varma, M., Saab, K., Delbrouck, J.-B., Lee-Messer, C., Dunnmon, J., Zou, J., and Ré, C. Domino: Discovering systematic errors with cross-modal embeddings. *arXiv preprint arXiv:2203.14960*, 2022.
- Garg, S., Perot, V., Limtiaco, N., Taly, A., Chi, E. H., and Beutel, A. Counterfactual fairness in text classification through robustness. In *Proceedings of the AAAI/ACM Conference on AI, Ethics, and Society*, 2019.
- Ge, Y., Xu, J., Zhao, B. N., Itti, L., and Vineet, V. Dall-e for detection: Language-driven context image synthesis for object detection. *arXiv preprint arXiv:2206.09592*, 2022.
- Geirhos, R., Rubisch, P., Michaelis, C., Bethge, M., Wichmann, F. A., and Brendel, W. ImageNet-trained CNNs are biased towards texture; increasing shape bias improves accuracy and robustness. In *International Conference on Learning Representations*, 2018.
- Geirhos, R., Jacobsen, J.-H., Michaelis, C., Zemel, R., Brendel, W., Bethge, M., and Wichmann, F. A. Shortcut learning in deep neural networks. In *Nature Machine Intelligence*, 2020a.
- Geirhos, R., Meding, K., and Wichmann, F. A. Beyond accuracy: quantifying trial-by-trial behaviour of cnns and humans by measuring error consistency. In *Advances in Neural Information Processing Systems*. 2020b.
- Geirhos, R., Narayanappa, K., Mitkus, B., Thieringer, T., Bethge, M., Wichmann, F. A., and Brendel, W. Partial success in closing the gap between human and machine vision. *Advances in Neural Information Processing Systems*, 2021.
- Geirhos, R., Rubisch, P., Michaelis, C., Bethge, M., Wichmann, F. A., and Brendel, W. Imagenet-trained cnns are biased towards texture; increasing shape bias improves accuracy and robustness. In *International Conference on Learning Representations*, 2022.
- Goodfellow, I., Bengio, Y., and Courville, A. *Deep Learning*. MIT Press, 2016.
- Goodfellow, I. J., Shlens, J., and Szegedy, C. Explaining and harnessing adversarial examples. *arXiv preprint arXiv:1412.6572*, 2014.
- Gowal, S., Qin, C., Huang, P.-S., Cemgil, T., Dvijotham, K., Mann, T., and Kohli, P. Achieving Robustness in the Wild via Adversarial Mixing with Disentangled Representations. *arXiv preprint arXiv:1912.03192*, 2019.
- Harder, F., Asadabadi, M. J., Sutherland, D. J., and Park, M. Differentially private data generation needs better features. *arXiv preprint arXiv:2205.12900*, 2022.
- He, K., Zhang, X., Ren, S., and Sun, J. Deep residual learning for image recognition. *Proceedings of the IEEE Conference on Computer Vision and Pattern Recognition*, 2016.
- Hendrycks, D. and Dietterich, T. Benchmarking Neural Network Robustness to Common Corruptions and Perturbations. In *International Conference on Learning Representations*, 2018.
- Hendrycks, D., Zhao, K., Basart, S., Steinhardt, J., and Song, D. Natural adversarial examples. *arXiv preprint arXiv:1907.07174*, 2019.
- Hendrycks, D., Basart, S., Mu, N., Kadavath, S., Wang, F., Dorundo, E., Desai, R., Zhu, T., Parajuli, S., Guo, M., Song, D., Steinhardt, J., and Gilmer, J. The Many Faces of Robustness: A Critical Analysis of Out-of-Distribution Generalization. *arXiv preprint arXiv:2006.16241*, 2020.
- Heusel, M., Ramsauer, H., Unterthiner, T., Nessler, B., and Hochreiter, S. Gans trained by a two time-scale update rule converge to a local nash equilibrium. In *Advances in Neural Information Processing Systems*. 2017.
- Hinton, G., Deng, L., Yu, D., Dahl, G. E., Mohamed, A.-r., Jaitly, N., Senior, A., Vanhoucke, V., Nguyen, P., Sainath, T. N., and others. Deep neural networks for acoustic modeling in speech recognition: The shared views of four research groups. *IEEE Signal processing magazine*, (6), 2012.
- Hu, X., Gan, Z., Wang, J., Yang, Z., Liu, Z., Lu, Y., and Wang, L. Scaling up vision-language pre-training for image captioning. *arXiv preprint arXiv:2111.12233*, 2021.
- Jain, S., Lawrence, H., Moitra, A., and Madry, A. Distilling model failures as directions in latent space. *arXiv preprint arXiv:2206.14754*, 2022a.
- Jain, S., Salman, H., Khaddaj, A., Wong, E., Park, S. M., and Madry, A. A data-based perspective on transfer learning. *arXiv preprint arXiv:2207.05739*, 2022b.

- Jia, R. and Liang, P. Adversarial examples for evaluating reading comprehension systems. *arXiv preprint arXiv:1707.07328*, 2017.
- Kather, J. N., Ghaffari Laleh, N., Foersch, S., and Truhn, D. Medical domain knowledge in domain-agnostic generative ai. In *npj Digital Medicine*, 2022.
- Khosla, A., Zhou, T., Malisiewicz, T., Efros, A. A., and Torralba, A. Undoing the damage of dataset bias. In *European Conference on Computer Vision*, 2012.
- Kolesnikov, A., Beyer, L., Zhai, X., Puigcerver, J., Yung, J., Gelly, S., and Houlsby, N. Big transfer (bit): General visual representation learning. In *European conference on computer vision*, 2020.
- Krizhevsky, A., Sutskever, I., and Hinton, G. E. Imagenet classification with deep convolutional neural networks. In *Advances in neural information processing systems*, 2012.
- Kuehlikamp, A., Becker, B., and Bowyer, K. Gender-from-iris or gender-from-mascara? In *IEEE Winter Conference on Applications of Computer Vision*, 2017.
- Kurakin, A., Goodfellow, I., and Bengio, S. Adversarial examples in the physical world. *arXiv preprint arXiv:1607.02533*, 2016.
- Laidlaw, C., Singla, S., and Feizi, S. Perceptual Adversarial Robustness: Defense Against Unseen Threat Models. *arXiv preprint arXiv:2006.12655*, 2020.
- Lapuschkin, S., Waldchen, S., Binder, A., Montavon, G., Samek, W., and Muller, K.-R. Unmasking clever hans predictors and assessing what machines really learn. In *Nature Communications*, 2019.
- Mania, H., Miller, J., Schmidt, L., Hardt, M., and Recht, B. Model similarity mitigates test set overuse. In *Advances in Neural Information Processing Systems*. 2019.
- Mann, H. B. and Whitney, D. R. On a test of whether one of two random variables is stochastically larger than the other. *The annals of mathematical statistics*, pp. 50–60, 1947.
- Miller, G. A. Wordnet: a lexical database for english. *Communications of the ACM*, 1995.
- Perez, E., Huang, S., Song, F., Cai, T., Ring, R., Aslanides, J., Glaese, A., McAleese, N., and Irving, G. Red teaming language models with language models. *arXiv preprint arXiv:2202.03286*, 2022.
- Qiu, H., Xiao, C., Yang, L., Yan, X., Lee, H., and Li, B. SemanticAdv: Generating Adversarial Examples via Attribute-conditional Image Editing. *arXiv preprint arXiv:1906.07927*, 2019.
- Radford, A., Kim, J. W., Hallacy, C., Ramesh, A., Goh, G., Agarwal, S., Sastry, G., Askell, A., Mishkin, P., Clark, J., Krueger, G., and Sutskever, I. Learning Transferable Visual Models From Natural Language Supervision. *OpenAI Blog*, 2021.
- Ramesh, A., Dhariwal, P., Nichol, A., Chu, C., and Chen, M. Hierarchical text-conditional image generation with clip latents. *arXiv preprint arXiv:2204.06125*, 2022.
- Recht, B., Roelofs, R., Schmidt, L., and Shankar, V. Do ImageNet Classifiers Generalize to ImageNet? *arXiv preprint arXiv:1902.10811*, 2019.
- Ribeiro, M. T., Singh, S., and Guestrin, C. "why should i trust you?": Explaining the predictions of any classifier. *arXiv preprint arXiv:1602.04938*, 2016. URL <https://arxiv.org/pdf/1602.04938>.
- Ribeiro, M. T., Singh, S., and Guestrin, C. Semantically equivalent adversarial rules for debugging NLP models. In *Proceedings of the Annual Meeting of the Association for Computational Linguistics*, 2018.
- Ribeiro, M. T., Wu, T., Guestrin, C., and Singh, S. Beyond accuracy: Behavioral testing of NLP models with Check-List. In *Proceedings of the 58th Annual Meeting of the Association for Computational Linguistics*, 2020.
- Rombach, R., Blattmann, A., Lorenz, D., Esser, P., and Ommer, B. High-resolution image synthesis with latent diffusion models. In *Proceedings of the IEEE/CVF Conference on Computer Vision and Pattern Recognition*, 2022.
- Sagawa, S., Koh, P. W., Hashimoto, T. B., and Liang, P. Distributionally robust neural networks for group shifts: On the importance of regularization for worst-case generalization. *arXiv preprint arXiv:1911.08731*, 2020.
- Saharia, C., Chan, W., Saxena, S., Li, L., Whang, J., Denton, E., Ghasemipour, S. K. S., Ayan, B. K., Mahdavi, S. S., Lopes, R. G., Salimans, T., Ho, J., Fleet, D. J., and Norouzi, M. Photorealistic text-to-image diffusion models with deep language understanding. *arXiv preprint arXiv:2205.11487*, 2022.
- Selvaraju, R. R., Cogswell, M., Das, A., Vedantam, R., Parikh, D., and Batra, D. Grad-cam: Visual explanations from deep networks via gradient-based localization. *arXiv preprint arXiv:1610.02391*, 2019.
- Song, Y., Shu, R., Kushman, N., and Ermon, S. Constructing unrestricted adversarial examples with generative models. In *Advances in Neural Information Processing Systems*, 2018.

- Steiner, A., Kolesnikov, A., Zhai, X., Wightman, R., Uszkor-eit, J., and Beyer, L. How to train your vit? data, augmentation, and regularization in vision transformers. *Transactions on Machine Learning Research*, 2022.
- Szegedy, C., Zaremba, W., Sutskever, I., Bruna, J., Erhan, D., Goodfellow, I., and Fergus, R. Intriguing properties of neural networks. *arXiv preprint arXiv:1312.6199*, 2013.
- Szegedy, C., Liu, W., Jia, Y., Sermanet, P., Reed, S., Anguelov, D., Erhan, D., Vanhoucke, V., and Rabinovich, A. Going deeper with convolutions. In *Proceedings of the IEEE/CVF Conference on Computer Vision and Pattern Recognition*, 2015.
- Szegedy, C., Ioffe, S., Vanhoucke, V., and Alemi, A. A. Inception-v4, inception-resnet and the impact of residual connections on learning. In *Thirty-first AAAI conference on artificial intelligence*, 2017.
- Torralba, A., Efros, A. A., and others. Unbiased look at dataset bias. In *Proceedings of the IEEE/CVF Conference on Computer Vision and Pattern Recognition*, 2011.
- Witteveen, S. and Andrews, M. Paraphrasing with large language models. *arXiv preprint arXiv:1911.09661*, 2019.
- Wong, E. and Kolter, J. Z. Learning perturbation sets for robust machine learning. In *International Conference on Learning Representations*, 2021.
- Xiao, C., Li, B., Zhu, J.-Y., He, W., Liu, M., and Song, D. Generating adversarial examples with adversarial networks. *arXiv preprint arXiv:1801.02610*, 2018.
- Xiao, K., Engstrom, L., Ilyas, A., and Madry, A. Noise or Signal: The Role of Image Backgrounds in Object Recognition. *arXiv preprint arXiv:2006.09994*, 2020.

A. Prompting the image-to-text model

To ensure that captions are descriptive and composed of short sentences, we prompt our image-to-text model with the following for all experiments:



is a realistic picture of two penguins. They are holding hands. They are standing in front of the sea. The picture is mostly grey. The penguins are facing away from the camera. They take up most of the image.



is a portrait photograph of a famous person. She is wearing two necklaces. She has dark hair and is wearing makeup. She is facing the camera and the background is black.



is a cute photograph of three kittens. They are under a blanket. The background is blurred but it seems white and orange. The blanket is purple. The two cats on the right are orange and the one on the left is grey. The orange cats have open eyes and the grey cat has closed eyes. They are all super cute.



is a realistic photograph of a [label name]. [...]

These images are not from IMAGENET but downloaded from the web. Choosing these captions is only done once and then fixed for all experiments in the paper. We also set the decoding strategy to be *greedy* (as we did not observe significant improvements from using beam search). We highlight that any expert knowledge, if needed, is only required to annotate these three images. Compared to annotating a full test set, the cost is negligible.

B. Additional results

B.1. Open-ended failure search

Large scale experiments. Similarly to Fig. 3 and Table 1, Fig. 6 and Table 3 show failure cases automatically found by our pipeline for a RESNET-50 available on TF-HUB in a fully open-ended manner (i.e., without leveraging an external dataset). The labels considered are a subset of the 200 labels present in IMAGENET-A. We let the reader interpret these failure cases themselves. The failures are diverse and are due to different factors, such as: (i) misleading color patterns (e.g., sea anemone → daisy), (ii) spurious context (e.g., jeep → snowplow), (iii) missing knowledge (e.g., custard apple → mask), or (iv) hallucinations (e.g., feather boa → maltese dog).

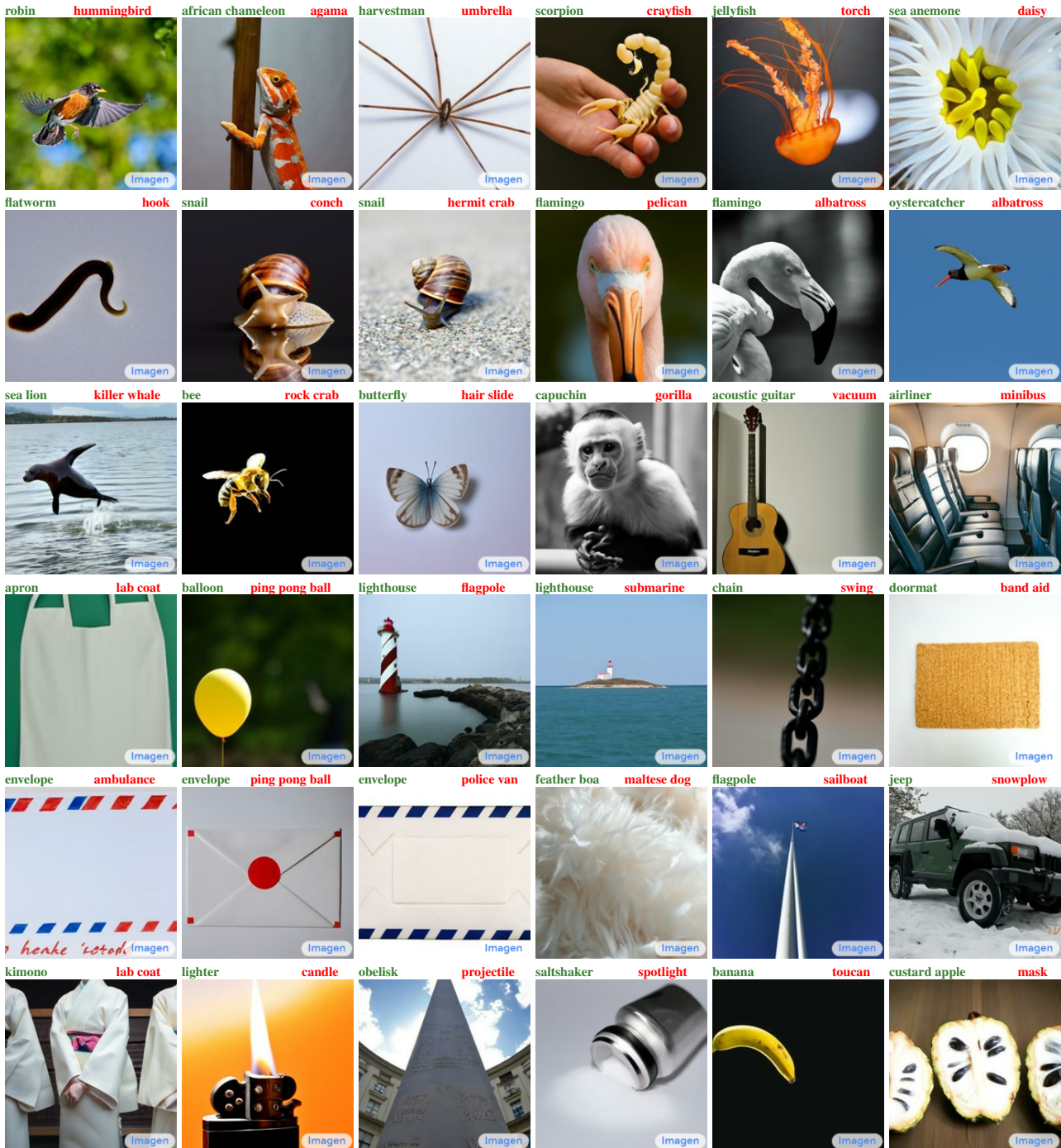


Figure 6. Illustration of failure cases listed in Table 3. The correct label is to the left in green. The incorrect prediction is to the right in red. The model used is a RESNET-50 found on TF-HUB.

Discovering Bugs in Vision Models using Off-the-shelf Image Generation and Captioning

True label	Target label	Caption	Failure rate (target)	
robin	hummingbird	a realistic photograph of a robin (oscine). — " — It is flying.	0.0032%	1×
african chameleon	agama	a realistic photograph of an african chameleon (lizard). — " — He is holding a stick. The chameleon is orange and white.	0.15%	1×
harvestman	umbrella	a realistic photograph of a harvestman (arthropod). — " — It is shot from above. The harvestman is on a white background.	1.01%	6.7×
scorpion	crayfish	a realistic photograph of a scorpion (arthropod). — " — It is on a person's hand.	0.45%	1×
jellyfish	torch	a realistic photograph of a jellyfish (invertebrate). — " — The background is black. The jellyfish is orange.	1.32%	2.9×
sea anemone	daisy	a realistic photograph of a sea anemone (coelenterate). — " — It is yellow and white. The background is blurred.	0.0042%	1×
flatworm	hook	a realistic photograph of a flatworm (invertebrate). — " — It is on a white background.	0.13%	29.5×
snail	conch	a realistic photograph of a snail (mollusk). — " — It is on a black background. The snail is reflected on the floor.	0.14%	1×
snail	hermit crab	a realistic photograph of a snail (mollusk). — " — It is on a grey road.	0.45%	3.2×
flamingo	pelican	a realistic photograph of a flamingo (aquatic bird). — " — It is a close up of the head. The flamingo is facing the camera.	0.32%	1×
flamingo	albatross	a realistic photograph of a flamingo (aquatic bird). — " — It is black and white. The flamingo is looking to the right.	1.33%	4.2×
oystercatcher	albatross	a realistic photograph of an oystercatcher (wading bird). — " — It is flying.	0.61%	1×
sea lion	killer whale	a realistic photograph of a sea lion (seal). — " — It is jumping out of the water.	1.58%	2.6×
bee	rock crab	a realistic photograph of a bee (insect). — " — It is flying. The background is black.	0.039%	1×
cabbage butterfly	hair slide	a realistic photograph of a cabbage butterfly (butterfly). — " — It is on a white background. It is in the middle of the image.	0.88%	22.5×
capuchin	gorilla	a realistic photograph of a capuchin (monkey). — " — It is a black and white photograph.	0.0082%	1×
acoustic guitar	vacuum	a realistic photograph of an acoustic guitar (stringed instrument). — " — It is leaning against a wall.	0.10%	12.2×
airliner	minibus	a realistic photograph of an airliner (heavier-than-air craft). — " — There are seats in the foreground.	0.023%	1×
apron	lab coat	a realistic photograph of an apron (clothing). — " — It is white.	0.87%	37.6×
balloon	ping-pong ball	a realistic photograph of a balloon (aircraft). — " — It is yellow. The background is blurred.	0.081%	1×
lighthouse	flagpole	a realistic photograph of a beacon (structure). — " — The lighthouse has red and white stripes.	1.30%	16.1×
lighthouse	submarine	a realistic photograph of a beacon (structure). — " — It is on a small island at the horizon.	0.0025%	1×
chain	swing	a realistic photograph of a chain (attachment). — " — The chain is vertical. The chain is in focus.	0.52%	208.2×
doormat	band aid	a realistic photograph of a doormat (floor cover). — " — The doormat is rectangular and is on a white background.	0.14%	1×
envelope	ambulance	a realistic photograph of an envelope (instrumentality). — " — It has white and has red and blue stripes at the top and bottom.	4.31%	31.3×
envelope	ping-pong ball	a realistic photograph of an envelope (instrumentality). — " — It is white and has a red dot on it.	0.086%	1×
envelope	police van	a realistic photograph of an envelope (instrumentality). — " — It has white and has white and blue diagonal stripes at the top and bottom.	0.18%	2.1×
feather boa	maltese dog	a realistic photograph of a feather boa (garment). — " — It is white and fluffy.	0.099%	1×
flagpole	sailboat	a realistic photograph of a flagpole (stick). — " — It is white and the sky is blue.	1.98%	20.0×
jeep	snowplow	a realistic photograph of a jeep (motor vehicle). — " — It is parked in the snow.	0.011%	1×
kimono	lab coat	a realistic photograph of a kimono (garment). — " — It is white.	0.84%	73.9×
lighter	candle	a realistic photograph of a lighter (instrumentality). — " — It has a flame coming out of it.	0.20%	1×
obelisk	projectile	a realistic photograph of an obelisk (structure). — " — It is pointing up. The sky is blue.	1.02%	5.0×
saltshaker	spotlight	a realistic photograph of a saltshaker (container). — " — It has a silver lid. The salt shaker is on a white background. The salt is spilling out of the jar.	0.16%	1×
banana	toucan	a realistic photograph of a banana (produce). — " — It is yellow and is floating in the air. The background is black.	3.05%	19.2×
custard apple	mask	a realistic photograph of a custard apple (produce). — " — The fruit is cut in half.	0.44%	1×
			3.57%	8.1×
			0.53%	1×
			17.86%	33.8×
			0.095%	1×
			2.12%	22.4×
			0.041%	1×
			12.5%	308.0×
			1.22%	1×
			12.5%	10.2×
			0.94%	1×
			5.68%	6.1×
			0.210%	1×
			17.86%	60.0×
			1.04%	1×
			75.%	72.0×
			0.510%	1×
			6.94%	11.7×
			4.59%	1×
			41.67%	9.1×
			0.19%	1×
			2.19%	11.5×
			0.30%	1×
			17.86%	59.3×
			0.69%	1×
			2.84%	4.1×
			5.37%	1×
			41.67%	7.8×
			0.14%	1×
			1.09%	7.7×
			1.02%	1×
			13.89%	13.7×
			0.0058%	1×
			0.047%	8.2×
			0.32%	1×
			4.46%	14.0×

Table 3. Absolute failure rates of a RESNET-50 for 36 additional true and target label pairs. We show the target failure rate (i.e., the model prediction is the target label). Captions are automatically discovered using the method detailed in Sec. 3. Note that to the contrary of Table 1, we consider an image to be misclassified when the top-1 prediction is wrong (and not from the same WORDNET parent) rather than when the true label is not part of the top-3 predictions.

Generalization to other vision architectures. We investigate whether our approach extends to other, more challenging backbones, such as a ViT-B/32 and ViT-B/8 which obtain much better performance than a RESNET50 on IMAGENET. We use the `fly` and `bee` failure case as our case study and run the same experiment as the one presented in Table 1. Results are reported in Table 4. First, we observe that both ViT models exhibit the same bias than the one found for the RESNET-50 model (that a fly on a flower is more often confused as a bee). Second, while the failure rates increase significantly compared to the baseline, the bias seems to be less pronounced (with only a $114\times$ and $13.5\times$ increase in failure rates compared to $497\times$ for the RESNET) which highlights the qualities of both models.

Architecture	True label	Target label	Caption	Failure rate (target)
ViT-B/32	fly	bee	a realistic photograph of a fly (insect).	0.0002% $1\times$
			— ” — it is on a flower.	0.02278% $113.9\times$
ViT-B/8	fly	bee	a realistic photograph of a fly (insect).	0.0002% $1\times$
			— ” — it is on a flower.	0.0027% $13.5\times$

Table 4. Absolute failure rates of a ViT-B/8, ViT-B/32 on the `fly/bee` failure case. We show the target failure rate (i.e., the model prediction is the target label). Captions are automatically discovered using the method detailed in Sec. 3.

Generalization to images from Google Image Search. We expand on the analysis in the main text on how failures transfer to images downloaded through *Google Image Search* by exploring results on additional prompts. For each prompt in Table 3, we query *Google Image Search* and automatically download the first 100 images (if we download too many images, the later, less relevant images may fail to capture the prompt). We take five pretrained RESNET-50s and measure the confusion rate for the target class on these images in Table 5. The results demonstrate that the failures we found with generated data generalize to real images. For the other prompts (not shown in Table 5), we found that the target failure rate is zero both for the original and modified prompt. This is presumably because there were not enough images to surface the failure rate. This demonstrates an additional benefit of our approach: we are not limited by images that exist on the web or are retrievable through an image search engine.

True label	Target label	Caption	Failure rate (target)
robin	hummingbird	a realistic photograph of a robin (oscine). — ” — It is flying.	$1.10\% \pm 1.10$ $10.31\% \pm 3.85$
african chameleon	agama	a realistic photograph of an african chameleon (lizard). — ” — He is holding a stick. The chameleon is orange and white.	$1.70\% \pm 0.59$ $4.35\% \pm 0.77$
scorpion	crayfish	a realistic photograph of a scorpion (arthropod). — ” — It is on a person’s hand.	$0.21\% \pm 0.46$ $0.67\% \pm 1.01$
lighthouse	submarine	a realistic photograph of a beacon (structure). — ” — It is on a small island at the horizon.	$0.38\% \pm 0.85$ $2.68\% \pm 0.56$
jeep	snowplow	a realistic photograph of a jeep (motor vehicle). — ” — It is parked in the snow.	$5.84\% \pm 1.23$ $21.89\% \pm 4.30$
lighter	candle	a realistic photograph of a lighter (instrumentality). — ” — It has a flame coming out of it.	$0.65\% \pm 0.96$ $2.63\% \pm 1.86$

Table 5. Failure rates for images from *Google Image Search*. We report the mean and standard deviation of the target failure rate for the original and discovered captions over five randomly initialized RESNET-50s. We find that the failure rates go up with the modified caption if the failure rate is non zero initially.

Statistical significance of results. We further investigate the significance of the results on two of the open-ended failure cases in the main paper (the ones exhibiting larger failure rates). Here, we evaluate our RESNET-50 and generate samples until we either find 10 images that cause the classifier to mispredict the class towards the target class (using top-1 accuracy instead of the typical top-3 to allow us to run many experiments efficiently) or find no misclassification towards the target class within 20K samples. We report the failure rate for the original and discovered captions and compute p-values using the Mann-Whitney U test (Mann & Whitney, 1947) at a significance level of 0.005 to determine if the differences in failure rates are statistically significant. Results are in Table 6. As the p-values (0.00015 , $6.34 \cdot 10^{-5}$) are lower than 0.005, we

Discovering Bugs in Vision Models using Off-the-shelf Image Generation and Captioning

find a *significant* result that images of the discovered caption (e.g., "... crayfish (crustacean). it is in a net.") are more often misclassified for the target class (e.g., `chainlink fence`) than the original caption (e.g., "... crayfish (crustacean).").

True label	Target label	Caption	Failure rate (target)	p-value
fly	bee	a realistic photograph of a fly (insect). — ” — it is on a flower.	0.00% ± 0.00 0.58% ± 0.15	0.00015
crayfish	chainlink fence	a realistic photograph of a crayfish (crustacean). — ” — it is in a net.	0.00% ± 0.00 2.09% ± 0.56	$6.34 \cdot 10^{-5}$

Table 6. Significance of failure rates. We report the mean and standard deviation of the target failure rate for the original and discovered captions over ten runs. We then compute the p-value to determine if the difference in failure rates between the original and discovered caption is statistically significant. We do this for two failure cases and find that our results are statistically significant.

B.2. Additional comparisons on IN-G-RN, IN-G-VIT

Models considered. We collate a large set of models trained on IMAGENET with differing size, pretraining, augmentation, and architectures in addition to the two RESNETs and VITs we trained:

- VIT-B*, VIT-L*, VIT-S* (Dosovitskiy et al., 2020): VITs pretrained on IMAGENET21K.
- VIT-R* (Steiner et al., 2022): a hybrid VIT and RESNET model pretrained on IMAGENET21K.
- BIT* (Kolesnikov et al., 2020): BIT models pretrained either on IMAGENET21K (BIT-M *) or not pretrained (BIT-S *).
- INCEPTION_RESNET V2 (Szegedy et al., 2017): a hybrid INCEPTION, RESNET model with no pretraining.
- INCEPTION* (Szegedy et al., 2015): INCEPTION models with no pretraining.
- RESNET* (He et al., 2016): RESNET models with no pretraining.

Transferability of errors on IN-G-RN and IN-G-VIT. We evaluate how often failures in IN-G-RN and IN-G-VIT transfer to these models in Fig. 7. We can see that failures from both IN-G-RN and IN-G-VIT transfer across model architectures. However, the VITs and BITS which are pretrained on IMAGENET21K and achieve lower error on IMAGENET are fooled the least often. Within a model class, larger versions of the model seem more robust. For example, VIT-B/16 is more robust than VIT-B/32 and similarly the larger BITS (those of size 101x1) are more robust than their smaller counterparts (those of size 50x1). Thus, stronger pretraining and larger models seem to lead to improved (but not complete) robustness against these generated datasets.

Error consistency on IN-G-RN and IN-G-VIT. Finally, we measure the error consistency of the models in Fig. 8. We combine IN-G-RN and IN-G-VIT into one dataset and evaluate how often models make similar errors while accounting for the accuracy of each model (see Eq. 3 in Geirhos et al., 2021). A value of 100% indicates that the errors two models make are perfectly correlated and -100% that they are perfectly anti-correlated. It is striking that errors are most consistent within

IN-G-RN1	39%	53%	34%	35%	63%	56%	49%	50%	46%	39%	51%	41%	63%	60%	62%	66%	60%	61%	77%	73%	69%	69%	69%	75%	70%	71%	75%	100%	78%	59%	54%
IN-G-VIT1	50%	61%	44%	45%	67%	62%	56%	61%	55%	49%	59%	51%	69%	70%	71%	70%	68%	68%	77%	76%	74%	73%	74%	77%	74%	76%	77%	79%	77%	100%	77%
ImageNet	5%	8%	4%	4%	7%	7%	5%	7%	9%	8%	11%	8%	13%	11%	12%	13%	11%	10%	14%	11%	14%	12%	12%	14%	13%	12%	14%	11%	10%	6%	6%
	VIT-B/16	VIT-B/32	VIT-B/8	VIT-L/16	VIT-R26-S/32 (light aug)	VIT-R26-S/32 (med. aug)	VIT-R50-L/32	VIT-S/16	BIT-M (101x1)	BIT-M (101x3)	BIT-M (50x1)	BIT-M (50x3)	BIT-S (101x1)	BIT-S (101x3)	BIT-S-r152x4	BIT-S (50x1)	BIT-S (50x3)	Inception_ResNet V2	Inception V1	Inception V2	Inception V3	ResNet101 V1	ResNet152 V1	ResNet50 V1	ResNet101 V2	ResNet152 V2	ResNet50 V2	RN1	RN2	VIT1	VIT2

Figure 7. Failure rates (top-3) for different models on two generated datasets and IMAGENET. We report the failure rates of different models trained on IMAGENET on both IN-G-RN and IN-G-VIT as well as IMAGENET.

Discovering Bugs in Vision Models using Off-the-shelf Image Generation and Captioning

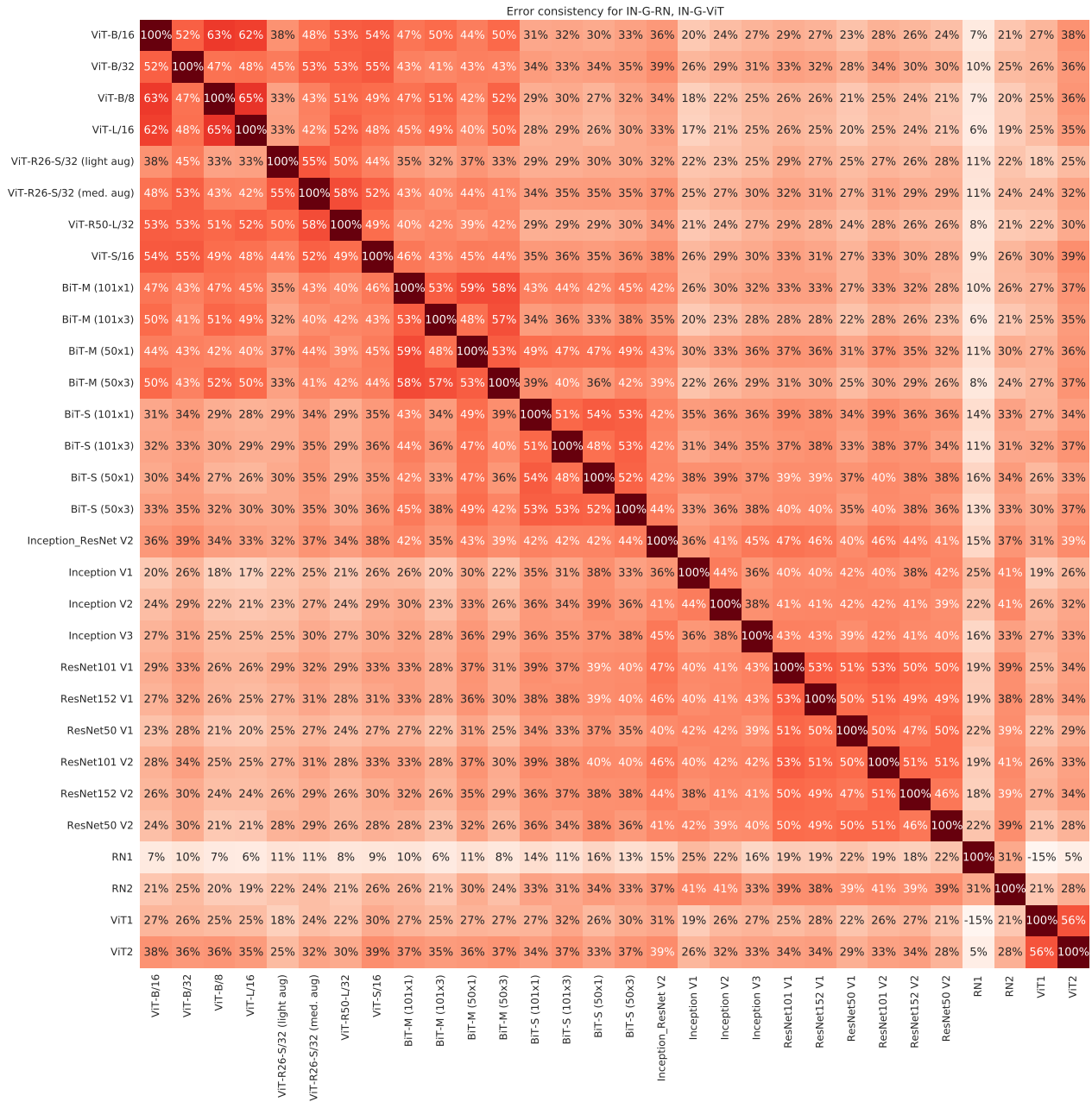


Figure 8. Error consistency for all models on the combined IN-G-RN and IN-G-VIT dataset.

a model class: RESNETS make similar errors to other RESNETS trained in a similar manner and similarly BITS make similar errors to other BITS, especially BITS trained in the same manner.

B.3. Reliability of the text-to-image model

We measured the error rate of our text-to-image model on all 200 labels present in ImageNet-A by generating 10 images per class (totalling 2000 images). We note that in our pipeline we only consider egregious errors as wrong (where the classifier top-3 does not include the correct label or any label under the same WordNet parent). Of the generated images, 3.95% did not represent the correct label and 1.45% showed an item from the wrong WordNet family (e.g., asking for an ocarina sometimes generated a maraca - both are musical instruments but only the ocarina is a wind instrument). Only a single class (porcupine) was systematically misrepresented. This experiment demonstrates that in general the text-to-image model is reliable and generates images of the right class.

C. Interpreting failure cases

In this section, we aim at further characterizing failure cases by investigating why the models considered in our work yield wrong predictions on IN-G-RN and IN-G-VIT instances. For that, we compared a few failure cases with their respective nearest neighbors within the training set of IMAGENET in order to find patterns that shed light on the reasons behind wrong predictions.

We find the ten nearest neighbors of an IN-G-VIT instance in the embedding space induced by the second-to-last layer of a VIT trained on IMAGENET, using cosine similarity as the distance measure. This particular model achieves 82.7% top-1 accuracy on the IMAGENET validation set and has a failure rate of 100% on IN-G-VIT.

Fig. 9-11 show IN-G-VIT failure cases, along with their respective ten nearest neighbors within the *full* IMAGENET training set and the ten nearest neighbors with the same label. Results suggest that failure cases found by our approach induce errors by generating images that have elements in their background which are more often found in other classes within IMAGENET. We further observe that all failure cases are closer to examples containing objects semantically related with cues present in images that are not commonly found in the training set of IMAGENET for these classes. In Fig. 9(a), for example, we show a failure case labeled as `mushroom` for which the VIT predicts the label `snail`. All nearest neighbors shown in Fig. 9(b) are labeled as `snail` and contain elements such as human skin and grass in the background, which do not appear in the nearest neighbors from the label `mushroom`, as shown in Fig. 9(c). The VIT appears to be capturing spurious features in its representations (presence of human skin and grassy background) and relying on them to make predictions, which lead it to yield the wrong label for the IN-G-VIT instance presented in Fig. 9(a). In Fig. 10 and 11, we observe a similar pattern, where the VIT focuses on spurious cues such as the presence of a net in the background in Fig. 10(a) and snow in Fig. 11(a). Exploiting such correlations made the model mistake the particular instances of `cabbage` `butterfly` and `flagpole` as `barn spider` and `ski`, respectively.



(a) IN-G-VIT failure case.



(b) 10 nearest neighbors of (a) in the IMAGENET train set.



(c) 10 nearest neighbors of (a) in the IMAGENET train set and in its respective label (mushroom).

Figure 9. Interpreting failure cases by inspecting nearest neighbors in the train set of IMAGENET. We analyze the failure case in IN-G-VIT shown in panel (a). The example is labeled as *mushroom* and classified as *snail* by a VIT trained on IMAGENET. In panel (b), we show the 10 nearest neighbors of (a) in the train set of IMAGENET. All 10 neighbors are from the class *snail* and have similar features to the failure case, such as the background (e.g., the human hand), while the 10 nearest neighbors with the label *mushroom* showed in panel (c) do not have those features. This suggests that the VIT correlates such features with the label *snail*, and these spurious correlations likely induced it to misclassify the image in (a).



(a) IN-G-VIT failure case.



(b) 10 nearest neighbors of (a) in the IMAGENET train set.

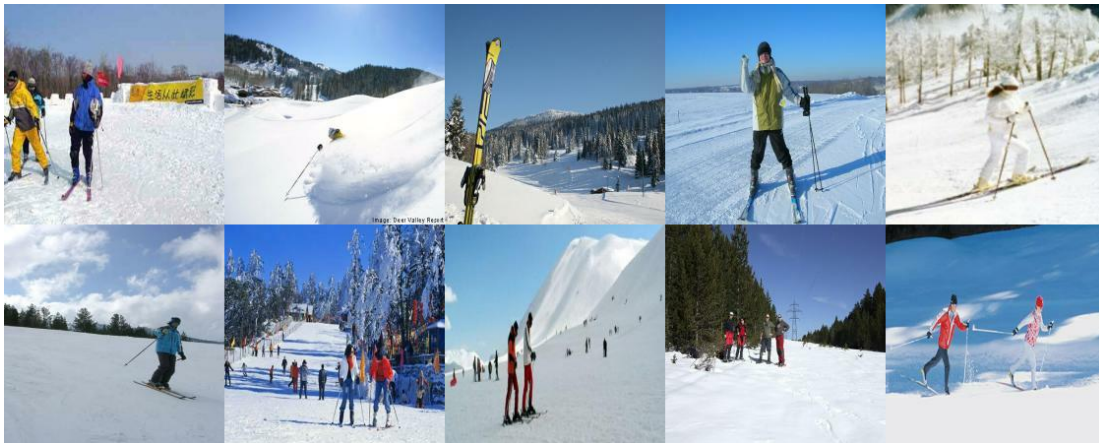


(c) 10 nearest neighbors of (a) in the IMAGENET train set and in its respective class (cabbage butterfly).

Figure 10. Interpreting failure cases by inspecting their nearest neighbors in the train set of IMAGENET. We analyze the failure case in IN-G-VIT shown in panel (a). The example is labeled as `cabbage butterfly` and classified as `barn spider` by a VIT trained on IMAGENET. In panel (b) we show the 10 nearest neighbors of (a) in the train set of IMAGENET. All 10 neighbors are from the classes `barn spider` or `black and gold garden spider` and have similarities to the failure case such as the white net in the background, while the 10 nearest neighbors in the class `cabbage butterfly` shown in panel (c) do not present those common features. This suggests that the VIT correlates such features with instances from the labels `barn spider` and `black and gold garden spider`, and exploiting these spurious correlations likely induced the model to misclassify the image in (a).



(a) IN-G-VIT failure case.



(b) 10 nearest neighbors of (a) in the IMAGENET train set..



(c) 10 nearest neighbors of (a) in the IMAGENET train set and in its respective class (flagpole)

Figure 11. Interpreting failure cases by inspecting their nearest neighbors in the train set of IMAGENET. We analyze the failure case in IN-G-VIT shown in panel (a). The example is labeled as `flagpole` and classified as `ski` by a VIT trained on IMAGENET. In panel (b) we show the 10 nearest neighbors of (a) in the train set of IMAGENET. All 10 neighbors have the label `ski` and have similarities to the failure case, such as simultaneously having snow on the ground and blue sky in the background, while the 10 nearest neighbors with the label `flagpole` shown in (c) do not present those common features. This suggests that the VIT correlates such features with instances from the label `ski`, and exploiting such spurious correlations likely induced it to misclassify the image in (a).

D. Malicious usage and mitigation strategies

This work demonstrates how to find failure cases in vision classifiers with the help of large-scale generative models. Much like adversarial examples (Biggio et al., 2013; Szegedy et al., 2013), malicious actors could leverage the proposed approach to build adversarial images that bypass automated online filtering mechanism. In this section, we discuss how to make classifiers robust to these failure cases.

First, classifiers can be trained with discovered failure cases to make them more robust to generated inputs. As a demonstration, we split the IN-G-VIT dataset into a train and test set (80% train, 20% test). We train the original VIT model in the exact same manner as before, except that batches are now made of 95% IMAGENET data and 5% IN-G-VIT data. We report results with and without additional synthetic data in Table 7. Training with additional generated data leads to a minimal loss of performance on IMAGENET while achieving nearly 90% top-1 accuracy on the IN-G-VIT test set. This demonstrates that adding the generated failure cases into the training set is an effective mitigation strategy.

Second, we note that our approach is computationally expensive. It requires hundreds to thousands of calls to the generative model and vision classifier to find a *single* failure case. Hiding the underlying classifier behind a rate-limited API can act as a first line of defense.

Training Set	top-1 on IMAGENET \uparrow	top-1 on IN-G-VIT \uparrow
IMAGENET (train)	82.57 \pm 0.09	5.60 \pm 2.80
IMAGENET (train) + IN-G-VIT (train)	82.11 \pm 0.05	88.11 \pm 0.44

Table 7. **top-1 accuracy on IMAGENET and IN-G-VIT.** We train a VIT model on either just IMAGENET or IMAGENET and IN-G-VIT. By training on IN-G-VIT, we achieve nearly 88% top-1 accuracy on IN-G-VIT (test) while minimally hurting performance on IMAGENET. To obtain standard deviations, we run the experiment with 5 random seeds.

E. Additional visualizations



Figure 12. **Images from the text-to-image model used in this manuscript.** Images are generated with captions identical to those used in Fig. 3(b) and Fig. 3(c). A comparison with DALL·E 2 is shown in Fig. 13.



Figure 13. **DALL·E 2 images.** Images are generated with captions identical to those used in Fig. 3(b) and Fig. 3(c). A comparison with the text-to-image model used in the paper is shown in Fig. 12.



Figure 14. **STABLE-DIFFUSION images.** Images are generated with captions identical to those used in Fig. 3(b) and Fig. 3(c). A comparison with the text-to-image model used in the paper is shown in Fig. 12.

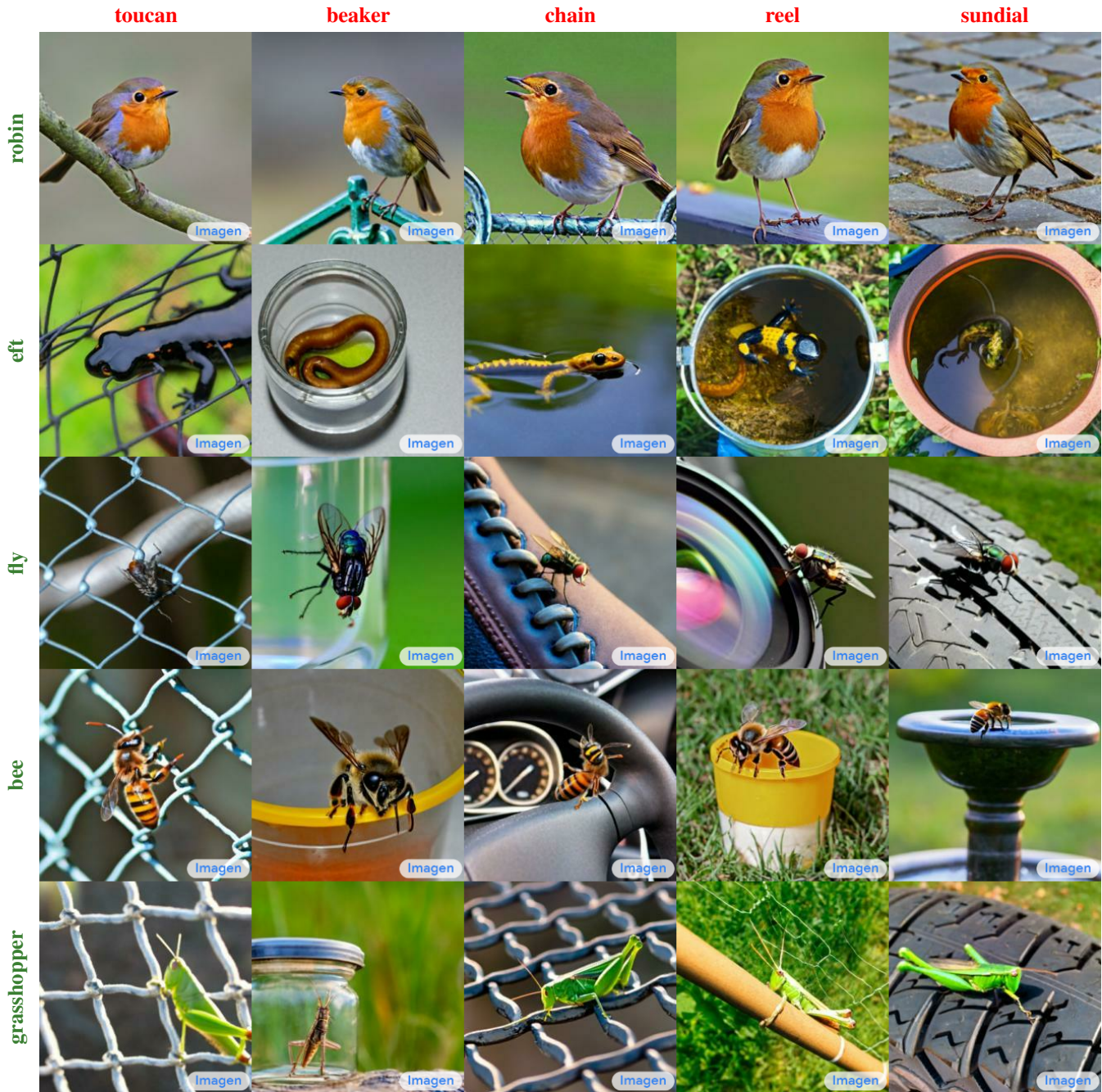


Figure 15. Further examples from IN-G-RN. The label at the top of the column is one of the incorrectly predicted top-3 labels and the label on the left is the true label.

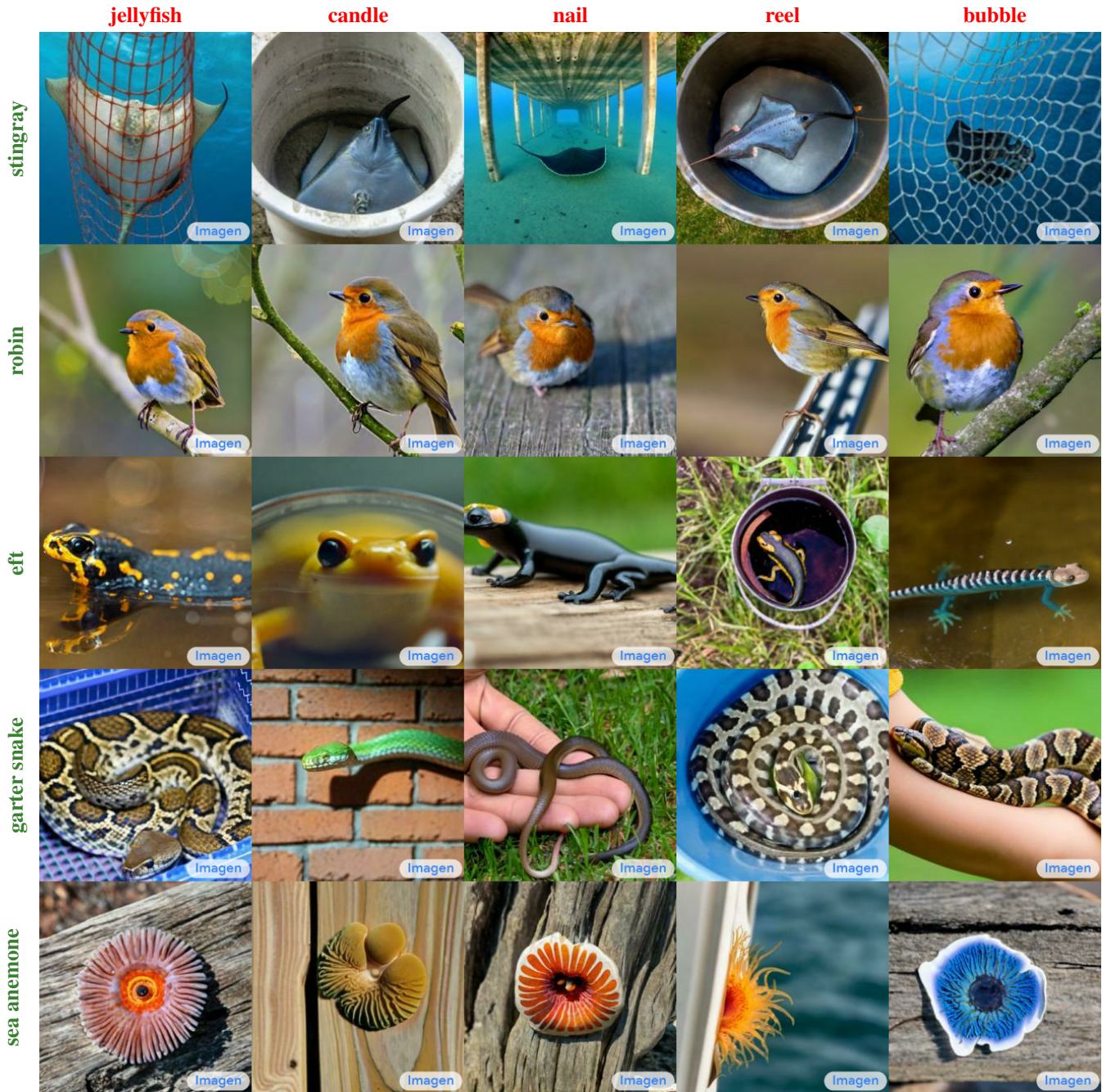


Figure 16. Examples from IN-G-VIT. The label at the top of the column is one of the incorrectly predicted top-3 labels and the label on the left is the true label.